CARBON 92 (2015) 339–347

Available at www.sciencedirect.com

ScienceDirect

journal homepage: www.elsevier.com/locate/carbon

Thiourea sole doping reagent approach for controllable N, S co-doping of pre-synthesized large-sized carbon nanospheres as electrocatalyst for oxygen reduction reaction

Jiangyao Chen [a,b], *Haimin Zhang* [a,c], *Porun Liu* [a], *Yibing Li* [a], *Guiying Li* [b], *Taicheng An* [b,*], *Huijun Zhao* [a,c,*]

[a] *Centre for Clean Environment and Energy, Griffith University, Gold Coast Campus, QLD 4222, Australia*

[b] *State Key Laboratory of Organic Geochemistry and Guangdong Key Laboratory of Environmental Protection and Resources Utilization, Guangzhou Institute of Geochemistry, Chinese Academy of Sciences, Guangzhou 510640, China*

[c] *Centre for Environmental and Energy Nanomaterials, Institute of Solid State Physics, Chinese Academy of Sciences, Hefei 230031, China*

ARTICLE INFO

Article history:
Received 15 January 2015
Accepted 27 April 2015
Available online 7 May 2015

ABSTRACT

The co-doping of heteroatoms into the pre-synthesized graphitic carbons normally requires the use of different doping reagents as heteroatom sources, leading to difficulties in controlling the contents of doped heteroatoms and their chemical bonding forms with graphitic structures. Graphitic carbon-based electrocatalysts with a relatively large size, rich microporous structure and high surface area could possess better structural stability and enhanced conductivity than those of small-sized carbon nanostructures (*e.g.*, nanodots). This study reported the use of a sole reagent (thiourea) as heteroatoms doping source to achieve controllable N, S co-doping of the pre-synthesized graphitic microporous carbon nanospheres (~100 nm in diameter) via a facial thermolysis process to produce high performance oxygen reduction reaction electrocatalysts. Results showed that the contents of the doped N, S and their chemical bonds with graphitic carbon structures could be simply controlled by controlling the thermolysis temperatures. With the experimental conditions investigated, the best performed electrocatalyst was obtained from 1100 °C doping process that possessed the most suitable N, S doping contents with 100% of doped N being in electrocatalytically active pyridinic-N and graphitic-N forms. The approach reported in this work could be useful for controllable heteroatoms co-doping of other types of new generation graphitic carbon materials.

* *Corresponding authors at:* State Key Laboratory of Organic Geochemistry and Guangdong Key Laboratory of Environmental Protection and Resources Utilization, Guangzhou Institute of Geochemistry, Chinese Academy of Sciences, Guangzhou 510640, China. Fax: +86 20 85290706 (T. An). Centre for Clean Environment and Energy, Griffith University, Gold Coast Campus, QLD 4222, Australia. Fax: +61 7 55528067 (H. Zhao).

E-mail addresses: antc99@gig.ac.cn (T. An), h.zhao@griffith.edu.au (H. Zhao).

http://dx.doi.org/10.1016/j.carbon.2015.04.090
0008-6223/

1. Introduction

Owing to unique physical and chemical properties, the new generation nanostructured carbon materials such as carbon nanotubes, graphene, carbon nanodots have been widely investigated for environmental and energy applications [1–3]. Recent years, the heteroatom (*e.g.*, N, B, S, P, I) doped graphitic carbon-based electrocatalysts have demonstrated as a class of promising alternatives to replace the expensive and scarce Pt-based electrocatalysts for oxygen reduction reaction (ORR) in fuel cells [4–7]. More recent studies have revealed that the ORR electrocatalytic activities of graphitic carbons could be further improved with co-doping of heteroatoms (*e.g.*, N, S etc.) due to the introduced synergetic effects of charge and spin densities changes [8,9]. To date, high temperature pyrolysis has been a general approach to realize the co-doping of heteroatoms into graphitic structures [10,11]. The majority of the reported heteroatom co-doped carbon materials by thermal treatment of pre-carbon structures such as carbon nanotubes and graphene in the presence of separated heteroatom containing precursors [12,13]. However, an intrinsic disadvantage of such co-doping approaches is the difficulty to precisely control the doping ratio and level of different heteroatoms, thus the ORR electrocatalytic activity [14]. Such a disadvantage could be overcome by employing a sole precursor containing the required heteroatom sources for co-doping. In this regard, our group recently demonstrated that well-controlled S and N co-doped graphitic carbon electrocatalyst can be readily obtained using a sole doping source of 1-allyl-2-thiourea [14].

To date, the reported heteroatom doped/co-doped carbon-based ORR electrocatalysts are mainly of carbon nanotubes, graphene, carbon nanodots and nanosheets [15–18], while barely any report is on the large-sized graphitic microporous carbon nanospheres (GMCNs). The large-sized GMCNs can provide better structural stability and electrical conductivity while maintain the large surface area and superior mass transport properties compared to small-sized carbon nanodots [3].

Herein, N, S co-doped graphitic microporous carbon nanospheres (NSGMCNs) were successfully fabricated using thiourea as a sole doping source in a facile thermolysis process under Ar atmosphere. The resultant NSGMCNs exhibit microporous structures with high surface areas. Importantly, the N and S doping ratio, level and even form in the carbon structure can be readily tuned by a simple control of thermolysis temperature. As an ORR electrocatalyst, the NSGMCNs sample with 1100 °C treatment exhibits the best ORR performance among all investigated electrocatalysts.

2. Experimental

2.1. Material synthesis

Graphitic microporous carbon nanospheres (GMCNs) with diameter of *ca.* 100 nm used in this work were initially synthesized by a previously reported method [19], followed by ultrasonically treated with mixed acid. Briefly, 0.6 g of phenol, 2.1 mL of formalin aqueous solution (37 wt%) and 15 mL of NaOH aqueous solution (0.1 M) were mixed and stirred at 70 °C for 0.5 h. After that, 0.96 g of triblock copolymer Pluronic F127 dissolved in 15 mL of deionized water was added. Then the mixture was stirred at 66 °C with a stirring speed of 340 ± 40 rpm for 2 h. After that, 50 mL of deionized water was added to dilute the solution. After reaction for another 16–18 h, 17.7 mL of the obtained solution was diluted with 56 mL of deionized water and kept at 130 °C for 24 h in a 100 mL Teflon lining autoclave reactor. The products were collected by centrifugation, washed several times with deionized water, dried at room temperature, carbonized at 700 °C in a N_2 atmosphere for 3 h and finally ultrasonically treated with a concentrated H_2SO_4/HNO_3 (3:1 with volume ratio) mixture solution in a water bath for 4 h.

To synthesize N, S co-doped GMCNs, 20 mg of acidification treated GMCNs was mixed with 20 mg of thiourea in 5 mL of deionized water. The mixture was ultrasonicated in a water bath for 0.5 h before continuously stirred for 3 h to facilitate the adsorption of thiourea onto the GMCNs surface. The thiourea/GMCNs composites were obtained *via* a slow evaporation process at 80 °C in an oven. The dried samples were subsequently calcinated at different temperatures (700, 800, 900, 1000, 1100 and 1200 °C) for 1 h with a ramp rate of 5 °C min^{-1} in an Ar atmosphere (denoted as NSGMCNs-700, NSGMCNs-800, NSGMCNs-900, NSGMCNs-1000, NSGMCNs-1100 and NSGMCNs-1200, respectively).

2.2. Characterization

The morphology and microstructure of the samples were obtained from scanning electron microscopy (SEM, JEOL JSM-6300F) and transmission electron microscopy (TEM, Philips F20). The Brunauer–Emmett–Teller (BET) method was utilized to calculate the specific surface areas using nitrogen adsorption–desorption isotherms of the samples on a Quantachrome Autosorb-1 equipment. Raman spectra were recorded on a Renishaw inVia Raman microscope with a laser excitation wavelength of 520 nm. Chemical compositions of the samples were analysed by X-ray photoelectron spectroscopy (XPS, Kratos Axis ULTRA incorporating a 165 mm hemispherical electron energy analyser). All binding energies were carefully aligned by reference to the C1s peak (284.6 eV) arising from surface hydrocarbons or possible adventitious hydrocarbon. The thermal processes of the sample was heated from 100 to 1000 °C with a heating rate of 5 °C min^{-1} at a flow rate of 40 mL min^{-1} in Ar atmosphere with simultaneous TG/DSC and online evolved gas analysis (TG/DSC-MS, Netzsch STA 449F3 equipment). Fourier transform infrared (FT-IR) spectroscopy analysis of the samples was performed using ALPHA FT-IR spectrometers with KBr as the reference sample.

Electrochemical measurements were carried out using a potentiostat (CHI 760D, CH Instrument, USA) with a conventional three-electrode cell: a working glassy carbon (GC) rotating disk electrode (RDE, 5.0 mm in diameter), an Ag/AgCl reference electrode and a Pt foil counter electrode. The catalyst ink was prepared by ultrasonically dispersing 1.0 mg of each grinded sample in 500 μL of solvent mixture of Nafion (5%), absolute ethanol and deionized water (V:V:V = 1:1:8) for 0.5 h. Then 12 μL suspension of each catalyst was pipetted onto the GC electrode surface and dry in a desiccator before use.

Cyclic voltammetry (CV) experiments were conducted in O_2 or N_2 saturated 0.1 M KOH solution with the scan rate of 100 mV s^{-1} in the potential range from −1.0 to +0.2 V at room temperature. Linear sweep voltammetry (LSV) measurements were performed on RDE in the O_2 saturated 0.1 M KOH solution at rotation rate varying from 250 to 2000 rpm and with the scan rate of 10 mV s^{-1}. The exact kinetic parameters including electron transfer number (n) and kinetic current density (J_K) were analyzed on the basis of Koutecky–Levich equations shown in Eqs. (1)–(3)[20].

$$\frac{1}{J}=\frac{1}{J_L}+\frac{1}{J_K}=\frac{1}{B\omega^{1/2}}+\frac{1}{J_K} \quad (1)$$

$$B=0.2nFC_0(D_0)^{2/3}v^{-1/6} \quad (2)$$

$$J_K=nFkC_0 \quad (3)$$

where J is the measured current density, J_K and J_L are the kinetic and diffusion limiting current densities, ω is the angular velocity of the disk ($\omega = 2\pi N$, N is the linear rotation speed), n is the overall number of electrons transferred in oxygen reduction, F is the Faraday constant (F = 96,485 C mol^{-1}), C_0 is the bulk concentration of O_2 ($C_0 = 1.2\times10^{-3}$ mol L^{-1}), v is the kinetic viscosity of the electrolyte (v = 0.1 m^2 s^{-1} in 0.1 M KOH), k is the electron transfer rate constant, and D_0 is the diffusion coefficient of O_2 in 0.1 M KOH ($D_0 = 1.9\times10^{-5}$ cm s^{-1}). The constant 0.2 is adopted when the rotating speed is expressed in rpm.

3. Results and discussion

Fig. 1A shows a typical SEM image of 1100 °C treated sample (NSGMCNs-1100) in the presence of thiourea under Ar atmosphere. It reveals carbon nanospheres with a uniform diameter of *ca.* 100 nm. Similar morphologies and size distributions can also be observed from the pristine carbon nanospheres (GMCNs) and samples treated with different thermolysis temperatures (Fig. S1), indicating high thermal stability of GMCNs. Importantly, the porous structures are clearly visible on the exposed nanosphere surface, implying an open pore structure. A typical TEM image of NSGMCNs-1100 shown in Fig. 1B further confirms the above observations. The N_2 adsorption–desorption isotherm of NSGMCNs-1100 shown in Fig. 1C reveals the measured isotherm with a type-I curve with a steeply increased adsorption at very low relative pressure, suggesting the presence of substantial micro-pore structures [21]. The amount of mesopores is limited as demonstrated by the gentle adsorption slope in the range of P/P_0 = 0.1–0.9 [22]. The hysteresis loop located at a higher pressure may reflect the interparticle texture between the carbon nanospheres [19]. An almost mono-distributed pore size of *ca.* 1.1 nm (Fig. 1D) is obtained from the analysis of the isotherm by a density functional theory model. The pristine GMCNs and other temperatures treated NSGMCNs also show similar N_2 adsorption–desorption isotherms (type-I) and pore size distributions (*ca.* 1.1 nm) as shown in Fig. S2A and S2B, indicating a microporous dominated pore structure for all samples investigated.

The above results suggest that the microporous structures are originated from the pristine carbon nanospheres and a

Table 1 – Surface areas of the synthesized samples.

Samples	Surface area (m^2 g^{-1})
GMCNs	240.7
NSGMCNs-700	602.3
NSGMCNs-800	665.1
NSGMCNs-900	725.2
NSGMCNs-1000	799.1
NSGMCNs-1100	855.1
NSGMCNs-1200	846.6

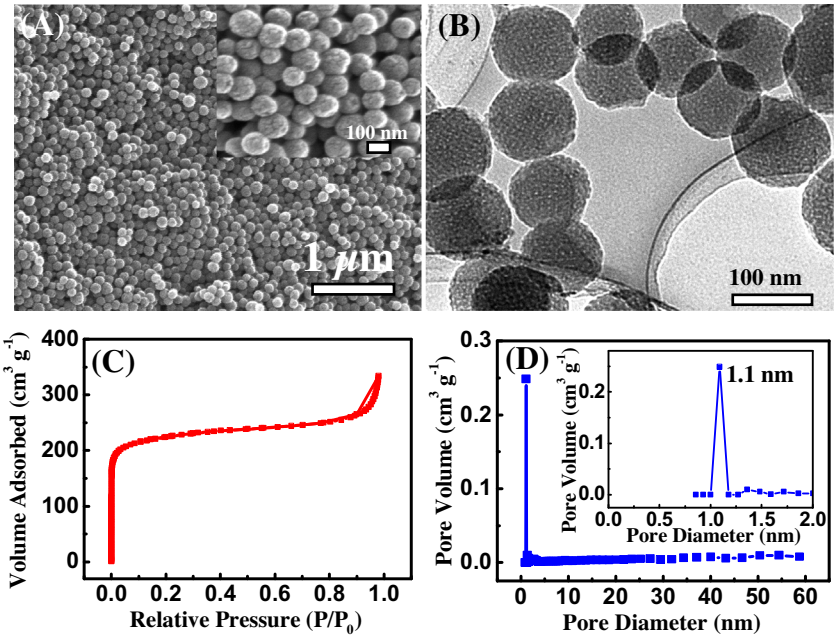

Fig. 1 – SEM (A), TEM (B) images, N_2 adsorption–desorption isotherm (C) and pore size distribution curve (D) of NSGMCNs-1100. (A colour version of this figure can be viewed online.)

Table 2 – Nitrogen and sulphur atomic percentage of various chemical states in prepared samples.

Samples	N/C (%)	Pyridinic N (%)	Pyrrolic N (%)	Graphitic N (%)	S/C (%)	N/S ratio
NSGMCNs-700	9.6	43.8	31.6	24.6	2.1	4.6
NSGMCNs-800	5.4	51.7	22.7	25.6	2.7	2.0
NSGMCNs-900	4.1	50.0	20.4	29.6	2.2	1.9
NSGMCNs-1000	2.8	43.0	17.0	40.0	2.1	1.3
NSGMCNs-1100	1.7	37.3	0	62.7	2.0	0.9
NSGMCNs-1200	1.4	0	0	100.0	1.1	1.3

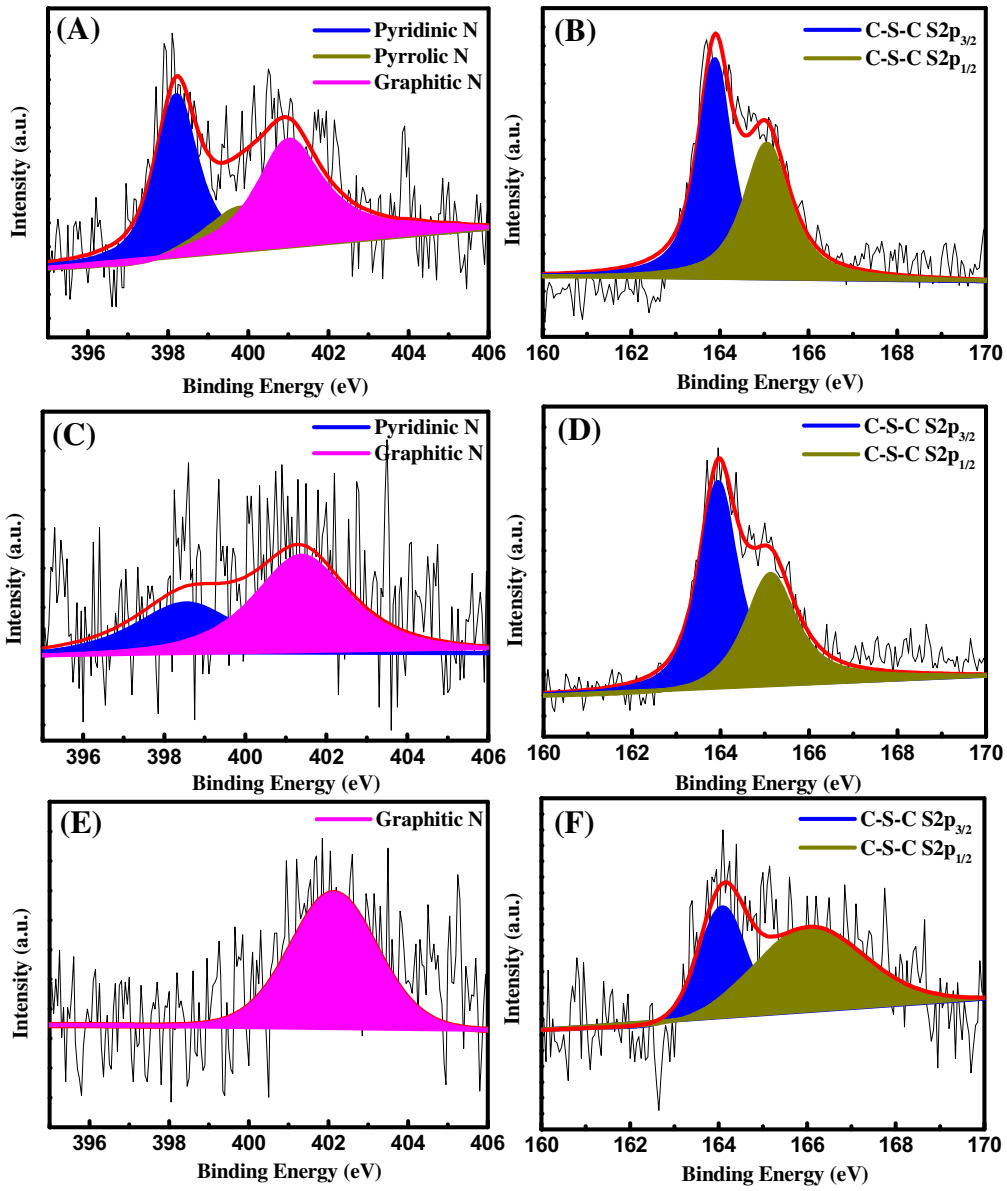

Fig. 2 – High resolution N1s and S2p spectra for NSGMCNs-1000 (A, B), NSGMCNs-1100 (C, D) and NSGMCNs-1200 (E, F). (A colour version of this figure can be viewed online.)

further thermolysis doping process has little effect on the pore structure of the original carbon nanospheres. The BET surface areas of GMCNs and NSGMCNs are listed in Table 1. It can be seen that the pristine GMCNs has a relatively low surface area of 240.7 $m^2 g^{-1}$. The surface area of the GMCNs is increased to 602.3 $m^2 g^{-1}$ after 700 °C treated for 1 h in the presence of thiourea (NSGMCNs-700). Such an increased trend for surface area can be retained up to 1100 °C (855.1 $m^2 g^{-1}$ for NSGMCNs-1100) then decreased slightly when the treatment temperature increases to 1200 °C (846.6 $m^2 g^{-1}$ for NSGMCNs-1200), which may be due to the microstructure damage of carbon nanospheres at higher

temperature. The large surface area (855.1 $m^2 g^{-1}$) of NSGMCNs-1100 is of advantageous for creating a larger number of surface catalytic active sites. Also, the formed porous structures of large-sized carbon nanospheres as electrocatalyst onto glassy carbon electrode can facilitate mass transfer to fully use these catalytic active sites for improving ORR performance.

Raman spectra of the as-synthesized NSGMCNs are obtained to indicate the degree of carbonization and surface defects of different temperature treated samples (Fig. S3). For all cases investigated, a typical D band centred at ~1350 cm^{-1} resulting from the breathing mode of aromatic rings known as the disorder or the defect band, and a G band centred at ~1590 cm^{-1} due to the bond stretching of the sp^2 carbon of a graphite phonon mode, are observed [23]. This result is consistent with typical Raman spectra of graphene oxides and reduced graphene oxides [23,24]. No significant shift or line broadening occurs, suggesting the surface structures of the carbon nanospheres are well maintained during the heteroatoms doping at different pyrolysis temperatures [25], which is in agreement with the SEM results. In addition, a continuous increased I_D/I_G ratio of higher temperature treated sample suggests an increased crystalline graphitic domain and number of structural defect sites at higher pyrolysis temperatures [8,10].

The composition and N, S doping level of the resultant NSGMCNs are investigated by XPS analyses. The XPS survey spectrum of the pristine GMCNs (Fig. S4) reveals only C1s and O1s peaks, while additional S2p, S2s, and N1s peaks are observed from the survey spectra of N, S co-doped NSGMCNs, indicating the successful incorporation of N and S into the carbon structures. The amount of doped N and S in the NSGMCNs is represented by N/C and S/C ratios and listed in Table 2. It was found that S/C ratio is between 2.0% and 2.7% for the samples obtained under the pyrolysis temperature ranged from 700 to 1100 °C, which then rapidly decreases to 1.1% for 1200 °C treated sample, indicating that the doped S is unstable under 1200 °C. In the case of N/C ratio, a continuous decreased trend (from 9.6% to 1.4%) is observed within the studied pyrolysis temperature range (from 700 to 1200 °C). Similar results have also been reported by others [26,27]. We and others have demonstrated the ORR performance of graphitic carbon-based electrocatalysts are not only significantly influenced by the ratios of N/C and S/C and their doping levels, but also by the types of N and S bonds (doped forms) with the graphitic carbon structures [8,14].

The N1s spectrum is used to determine the doped nitrogen forms. The presence of three common forms of doped N, pyridinic N, pyrrolic N and graphitic N can normally be confirmed by the appearance of the N1s spectrum fitting peaks at 398.0–398.9 eV, 400.0–400.3 eV and 401.0–402.0 eV, respectively [28,29]. As shown in Fig. 2 and Fig. S5, the forms of the doped N are very different for different temperature treated NSGMCNs. For NSGMCNs-700, pyridinic N, pyrrolic N and graphitic N account for 43.8%, 31.6% and 24.6% of the total N content, respectively (Table 2). As the temperature increases to 800 °C, the percentage of pyrrolic N decreases to 22.7% while that of pyridinic N and graphitic N increases to 51.7% and 25.6%, respectively. Similar results were also obtained by others [30]. Further increasing the temperature to 900 and 1000 °C, the pyridinic N and pyrrolic N are both decreased while graphitic N is increased, consistent with other reports [20,31]. Similar trends of change for three forms of doped N with pyrolysis temperatures equal to or lower than 1000 °C are also observed elsewhere [32,33]. When the pyrolysis temperature increases to 1100 °C, only the pyridinic N (37.3%) and graphitic N (62.7%) are presented in the sample (NSGMCNs-1100). Interestingly, the pyridinic N also disappears and only the graphitic N can be determined when the temperature reaches 1200 °C (NSGMCNs-1200). The above results demonstrate that the doped N form and level can be readily tuned by simply controlling the pyrolysis temperature.

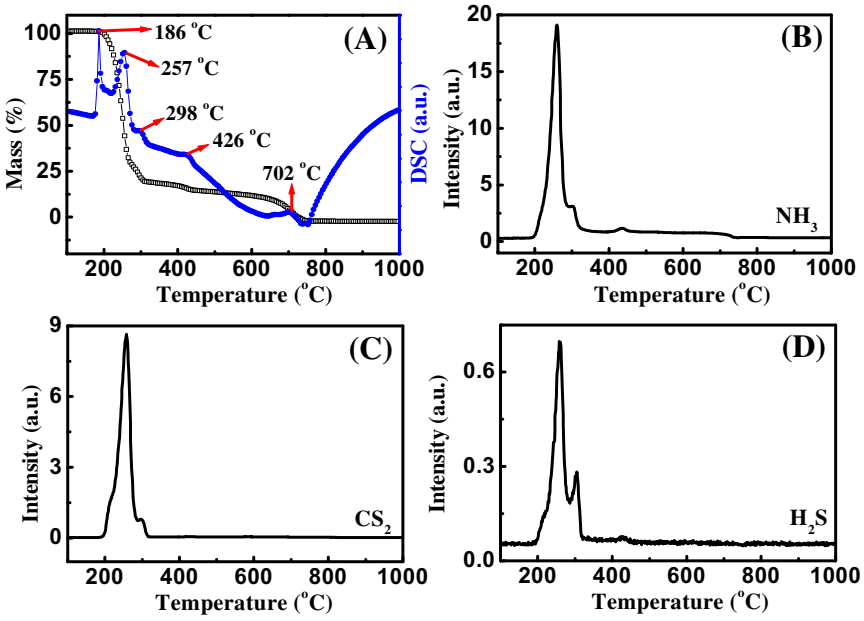

Fig. 3 – TG/DSC (A) and MS (B, C and D) curves of thiourea under Ar protection from 100 °C to 1000 °C, respectively. (A colour version of this figure can be viewed online.)

The high-resolution S2p XPS spectra of NSGMCNs are shown in Fig. 2 and Fig. S5. And the spectra of all samples can be fitted to two energy components ($S2p_{3/2}$ and $S2p_{1/2}$) that can be assigned to –C–S–C– type of bonds. FT-IR spectrum is also used in this work to characterize the chemical functional groups in NSGMCNs (Fig. S6). The disappearance of FT-IR peaks resulting from oxygen containing functional groups from the higher temperature treated samples suggests that the observed oxygen contents from the XPS spectra could be due to the adsorbed oxygen and water from the environment.

In order to better understand the formation process, thiourea was heated in Ar atmosphere and simultaneously monitored for TG/DSC and the evolved gaseous products (TG/DSC-MS) (Fig. 3). As shown in Fig. 3A, almost 80% weight loss of thiourea occurs in the temperature range of 100 to 310 °C, while complete decomposition occurs after 722 °C. As shown in Fig. 3, NH_3, CS_2 and H_2S start to emit when the temperature is higher than 186 °C. The emitted gases reach the maximum at 257 °C. When the temperature reaches 426 °C, a second emission process for NH_3 and H_2S is observed (Fig. 3B and 3D), while for NH_3, the third emission process is observed at 702 °C (Fig. 3B). Among the three determined N and S species, NH_3 should be responsible for the N doping, while CS_2 and H_2S should be the main contributors for S doping [34], but the contribution from CS_2 should be much greater than that of H_2S due to its significantly higher concentration.

To evaluate the ORR electrocatalytic performance of the prepared samples, CV experiments for NSGMCNs-1100 are firstly carried out in O_2 or N_2 saturated 0.1 M KOH solution at a scan rate of 100 mV s^{-1}, as shown in Fig. 4A. It can be found that within the potential range of −1.0 to +0.2 V, a featureless voltammetric response is observed in the N_2 saturated solution. In contrast, a well-defined cathodic current

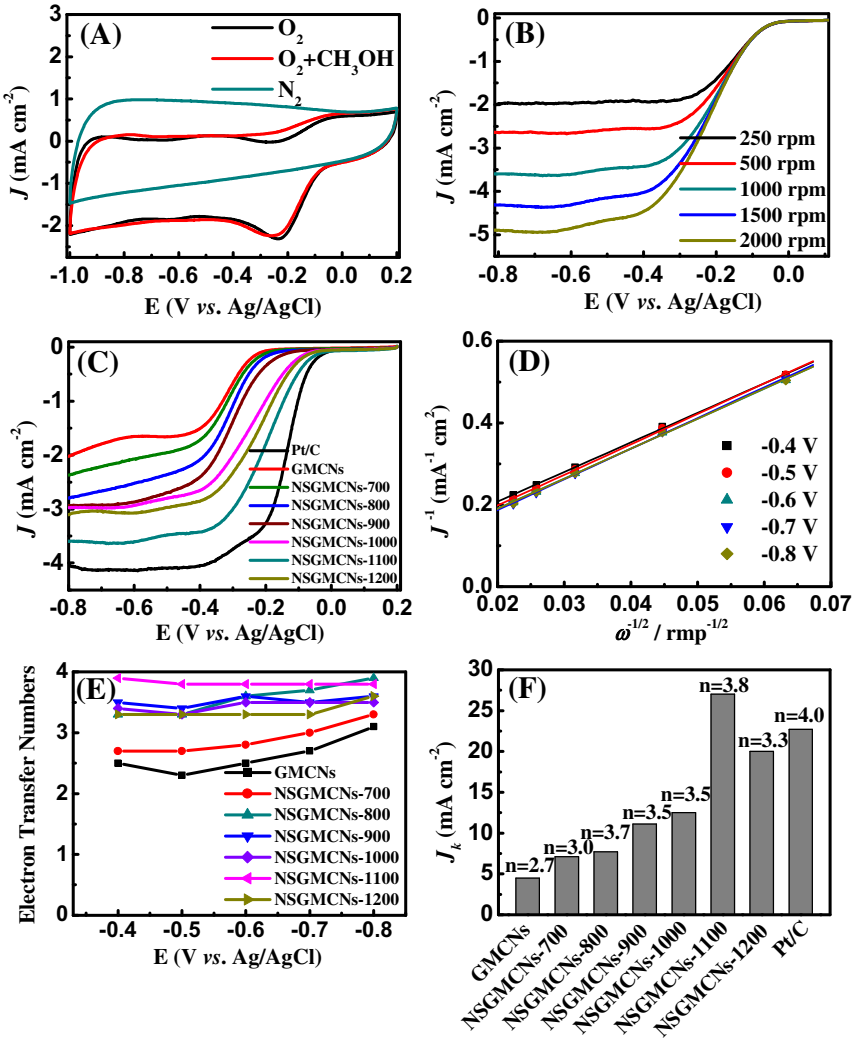

Fig. 4 – CV curves of NSGMCNs-1100 (A) electrode in an N_2 and O_2 saturated 0.10 M KOH solution or an O_2-saturated 0.1 M solution of KOH upon addition of 3 M methanol at a scan rate of 100 mV s^{-1}. (B) LSV curves obtained for NSGMCNs-1100 at various rotation rates. (C) LSV curves of GMCNs, NSGMCNs and Pt/C obtained with a RDE at 1000 rpm and 10 mV s^{-1}. (D) K–L plots for NSGMCNs-1100 obtained from LSV curves at different electrode potentials. (E) The corresponding electron transfer numbers for GMCNs and NSGMCNs at different electrode potentials. (F) Kinetic limiting current of GMCNs, NSGMCNs and Pt/C as well as the corresponding electron-transfer numbers at −0.7 V. (A colour version of this figure can be viewed online.)

peak cantered at −0.23 V is observed from the O_2 saturated solution, indicating a pronounced ORR electrocatalytic activity of NSGMCNs-1100. For comparison, CV curves in O_2 saturated solution for GMCNs and other temperatures treated samples are shown in Fig. S7. Clearly, larger cathodic current densities with anodically shifted peak potentials are observed with increased treatment temperature up to 1100 °C. However, a reversed trend is observed from the sample (NSGMCNs-1200) treated with 1200 °C. It is well known that the Pt/C electrocatalyst often suffers from the crossover effects of fuel molecules such as methanol. As shown in Fig. S8, the CV curve of the Pt/C electrode shows distinctive methanol oxidation peak with an addition of 3 M methanol. In contrast, no noticeable change can be observed from the NSGMCNs-1100 electrode under the same conditions (Fig. 4A), indicating that the NSGMCNs-1100 possesses an excellent selectivity towards ORR and high tolerance to the interference of fuel molecules than that of the commercial Pt/C catalyst. To gain further insight into the ORR process on the prepared NSGMCNs, the LSV experiments were conducted using NSGMCNs coated RDE at different rotating rates from 250 to 2000 rpm in a 0.1 M KOH solution saturated with O_2. As shown in Fig. 4B and Fig. S9, the oxygen reduction currents increase with increasing rotation rates for all the cases investigated. Moreover, NSGMCNs-1100 possesses the highest current density among other NSGMCNs.

The corresponding Koutecky–Levich (K–L) plots are obtained at different potentials and shown in Fig. 4D and Fig. S9. For all electrocatalysts investigated, good linearities over the potential range between −0.4 and −0.8 V were observed. The transferred electron numbers (n) determined from K–L equation for carbon nanosphere samples are shown in Fig. 4E. It was found that the measured transferred electron numbers for NSGMCNs-1100 are between 3.8 and 3.9, very consistent within the potential range investigated, indicating a desired four-electron ORR process. Fig. 4D and Fig. S9, also show that the K–L plots for NSGMCNs-1100 at different potentials from −0.4 V to −0.8 V are very close, indicating similar catalytic kinetic properties in the investigated potential range. However, the K–L plots of NSGMCNs catalysts obtained at low calcination temperatures (*e.g.*, from 700 to 1000 °C) are clearly differed from each other (Fig. S9). Nevertheless, the overall trend is that the K–L plots at different potentials become closer with further increasing calcination temperature, indicating significantly improved catalytic kinetic properties of the NSGMCNs catalysts with increased calcination temperature. However, a higher calcination temperature (*e.g.*, 1200 °C) may arouse the damage of carbon nanosphere structure, resulting in a decreased catalytic kinetic current density compared to NSGMCNs-1100. To avoid the unwanted effect of electrochemical reactions such as electrolysis of water, the kinetic current densities (J_K) at −0.7 V of all electrocatalysts investigated were calculated for meaningful comparison of their catalytic kinetic properties. The results demonstrate that the NSGMCNs-1100 exhibits the highest J_K value of 27.0 mA cm^{-2} among all electrocatalysts investigated, even higher than that of commercial Pt/C for which J_K = 22.7 mA cm^{-2} was observed (see Fig. 4F). It is known that a less cathodic onset potential indicates a lower ORR overpotential. Remarkably, the NSGMCNs-1100 shows the most positive ORR onset potential of *ca.* −0.07 V in comparison with other NSGMCNs, which is very close to the value of −0.06 V for Pt/C (Fig. 4C). The durability experiments are also carried out. The results reveal that 95% of the initial current density of NSGMCNs-1100 can be retained over the testing period, while for the Pt/C catalyst, only 73% of the initial current density can be retained under the same testing conditions (Fig. 5).

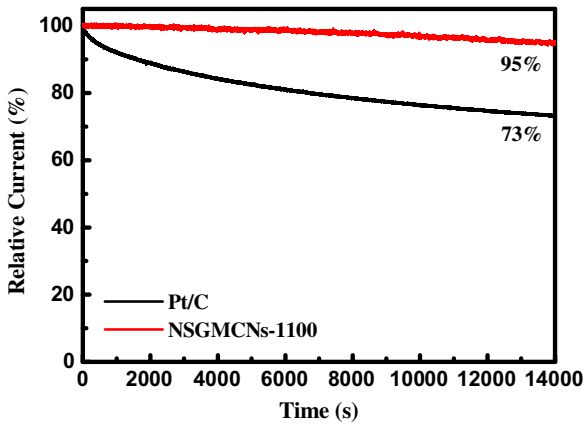

Fig. 5 – Durability evaluation of NSGMCNs-1100 and Pt/C electrodes for 14,000 s at −0.4 V and a rotation rate of 1000 rpm. (A colour version of this figure can be viewed online.)

The best ORR performance of NSGMCNs-1100 could be ascribed to the synergistic effect introduced by its large surface area and the most appropriate N, S doping level and doping forms [14]. As shown in Table 1, NSGMCNs-1100 possesses the highest surface area among all carbon nanosphere materials investigated, favourable for creating more catalytic active sites, thus improving ORR performance. Additionally, the formed porous structures between large-sized carbon nanospheres as electrocatalyst onto glassy carbon electrode can facilitate mass transfer, enabling the full utilisation of all catalytic active sites for superior ORR performance. Moreover, the N, S doping level of NSGMCNs-1100 is relatively low with a N/S ratio of *ca.* 0.9, which is the lowest and closest to the value of 1, implying that a superior graphitic ORR electrocatalysts should possess a relatively low but similar content ratio of doped N and S. Besides, the chemical bondings of the doped N and S with graphitic carbon structure can also influence the ORR performance of resultant NSGMCNs [8]. It has been confirmed that the pyridinic N and graphitic N are the most effective doping forms for enhancing the ORR catalytic activity of graphitic carbon-based electrocatalysts [29]. The best ORR performance of NSGMCNs-1100 could therefore be due to the appropriate N, S doping level and doping forms (*e.g.*, pyridinic N and graphitic N) to create more catalytic active sites. Importantly, the content of the ORR inactive form of pyrrolic N in NSGMCNs-1100 is essentially zero (Table 2), which could be another attribute for its superior ORR performance [14]. Additionally, the decreased ORR activity observed from the NSGMCNs-1200 could be due to the significantly reduced N, S doping level and decreased catalytic kinetic property.

4. Conclusions

In summary, we have successfully demonstrated that controllable N, S co-doping of pre-synthesized graphitic microporous carbon nanospheres to produce high performance ORR electrocatalysts could be achieved using a sole doping precursor containing both heteroatoms (*e.g.*, thiourea) via a facial thermal treatment process. The approach demonstrated in this work could be used as a generic method for controllable heteroatoms co-doping of other types of new generation graphitic carbon materials such as graphene and carbon nanotubes.

Acknowledgements

This work was financially supported by NSFC–Guangdong Joint Funds (U1401245), NSFC (21307132, 41373102, 51372248), National Natural Science Funds for Distinguished Young Scholars (41425015).

Appendix A. Supplementary data

Supplementary data associated with this article can be found, in the online version, at http://dx.doi.org/10.1016/j.carbon.2015.04.090.

REFERENCES

[1] An TC, Chen JY, Nie X, Li GY, Zhang HM, Liu XL, et al. Synthesis of carbon nanotube-anatase TiO_2 sub-micrometer-sized sphere composite photocatalyst for synergistic degradation of gaseous styrene. ACS Appl Mater Interfaces 2012;4(11):5988–96.
[2] Ma XL, Ning GQ, Sun YZ, Pu YJ, Gao JS. High capacity Li storage in sulfur and nitrogen dual-doped graphene networks. Carbon 2014;79:310–20.
[3] Zhang HM, Wang Y, Wang D, Li YB, Liu XL, Liu PR, et al. Hydrothermal transformation of dried grass into graphitic carbon-based high performance electrocatalyst for oxygen reduction reaction. Small 2014;10(16):3371–8.
[4] Yang Z, Nie HG, Chen X, Chen XH, Huang SM. Recent progress in doped carbon nanomaterials as effective cathode catalysts for fuel cell oxygen reduction reaction. J Power Sources 2013;236:238–49.
[5] You CH, Liao SJ, Li HL, Hou SY, Peng HL, Zeng XY, et al. Uniform nitrogen and sulfur co-doped carbon nanospheres as catalysts for the oxygen reduction reaction. Carbon 2014;69:294–301.
[6] Su YZ, Zhang Y, Zhuang XD, Li S, Wu DQ, Zhang F, et al. Low-temperature synthesis of nitrogen/sulfur co-doped three-dimensional graphene frameworks as efficient metal-free electrocatalyst for oxygen reduction reaction. Carbon 2013;62:296–301.
[7] Yang DS, Bhattacharjya D, Inamdar S, Park J, Yu JS. Phosphorus-doped ordered mesoporous carbons with different lengths as efficient metal-free electrocatalysts for oxygen reduction reaction in alkaline media. J Am Chem Soc 2012;134(39):16127–30.
[8] Liang J, Jiao Y, Jaroniec M, Qiao SZ. Sulfur and nitrogen dual-doped mesoporous graphene electrocatalyst for oxygen reduction with synergistically enhanced performance. Angew Chem Int Ed 2012;51(46):11496–500.
[9] Xu JX, Zhao Y, Shen C, Guan LH. Sulfur- and nitrogen-doped, ferrocene-derived mesoporous carbons with efficient electrochemical reduction of oxygen. ACS Appl Mater Interfaces 2013;5(23):12594–601.
[10] Zheng Y, Jiao Y, Ge L, Jaroniec M, Qiao SZ. Two-step boron and nitrogen doping in graphene for enhanced synergistic catalysis. Angew Chem Int Ed 2013;52(11):3110–6.
[11] Paraknowitsch JP, Thomas A. Doping carbons beyond nitrogen: an overview of advanced heteroatom doped carbons with boron, sulphur and phosphorus for energy applications. Energy Environ Sci. 2013;6(10):2839–55.
[12] Wang XW, Sun GZ, Routh P, Kim DH, Huang W, Chen P. Heteroatom-doped graphene materials: syntheses, properties and applications. Chem Soc Rev 2014;43(20):7067–98.
[13] Shi QQ, Peng F, Liao SX, Wang HJ, Yu H, Liu ZW, et al. Sulfur and nitrogen co-doped carbon nanotubes for enhancing electrochemical oxygen reduction activity in acidic and alkaline media. J Mater Chem A 2013;1(47):14853–7.
[14] Li YB, Zhang HM, Wang Y, Liu PR, Yang HG, Yao XD, et al. A self-sponsored doping approach for controllable synthesis of S and N co-doped trimodal-porous structured graphitic carbon electrocatalysts. Energy Environ Sci. 2014;7(11):3720–6.
[15] Wang CF, Sun D, Zhuo KL, Zhang HC, Wang JJ. Simple and green synthesis of nitrogen-, sulfur-, and phosphorus-co-doped carbon dots with tunable luminescence properties and sensing application. Rsc Adv. 2014;4(96):54060–5.
[16] Wang X, Wang J, Wang DL, Dou SO, Ma ZL, Wu JH, et al. One-pot synthesis of nitrogen and sulfur co-doped graphene as efficient metal-free electrocatalysts for the oxygen reduction reaction. Chem Commun 2014;50(37):4839–42.
[17] Zhao Y, Yang LJ, Chen S, Wang XZ, Ma YW, Wu Q, et al. Can boron and nitrogen co-doping improve oxygen reduction reaction activity of carbon nanotubes? J Am Chem Soc 2013;135(4):1201–4.
[18] Zheng RP, Mo ZY, Liao SJ, Song HY, Fu ZY, Huang PY. Heteroatom-doped carbon nanorods with improved electrocatalytic activity toward oxygen reduction in an acidic medium. Carbon 2014;69:132–41.
[19] Fang Y, Gu D, Zou Y, Wu ZX, Li FY, Che RC, et al. A low-concentration hydrothermal synthesis of biocompatible ordered mesoporous carbon nanospheres with tunable and uniform size. Angew Chem Int Ed 2010;49(43):7987–91.
[20] Liu RL, Wu DQ, Feng XL, Mullen K. Nitrogen-doped ordered mesoporous graphitic arrays with high electrocatalytic activity for oxygen reduction. Angew Chem Int Ed 2010;49(14):2565–9.
[21] Jin Z, Zhao HY, Zhao XJ, Fang QR, Long JR, Zhu GS. A novel microporous MOF with the capability of selective adsorption of xylenes. Chem Commun 2010;46(45):8612–4.
[22] Su YS, Manthiram A. Lithium-sulphur batteries with a microporous carbon paper as a bifunctional interlayer. Nat Commun 2012:3.
[23] Fang Y, Lv YY, Che RC, Wu HY, Zhang XH, Gu D, et al. Two-dimensional mesoporous carbon nanosheets and their derived graphene nanosheets: synthesis and efficient lithium ion storage. J Am Chem Soc 2013;135(4):1524–30.
[24] Eda G, Chhowalla M. Chemically derived graphene oxide: towards large-area thin-film electronics and optoelectronics. Adv Mater 2010;22(22):2392–415.
[25] Sheng ZH, Gao HL, Bao WJ, Wang FB, Xia XH. Synthesis of boron doped graphene for oxygen reduction reaction in fuel cells. J Mater Chem 2012;22(2):390–5.
[26] Iwazaki T, Yang HS, Obinata R, Sugimoto W, Takasu Y. Oxygen-reduction activity of silk-derived carbons. J Power Sources 2010;195(18):5840–7.

[27] Chen S, Bi JY, Zhao Y, Yang LJ, Zhang C, Ma YW, et al. Nitrogen-doped carbon nanocages as efficient metal-free electrocatalysts for oxygen reduction reaction. Adv Mater 2012;24(41):5593–7.
[28] Biddinger EJ, Ozkan US. Role of graphitic edge plane exposure in carbon nanostructures for oxygen reduction reaction. J Phys Chem C 2010;114(36):15306–14.
[29] Wang HB, Maiyalagan T, Wang X. Review on recent progress in nitrogen-doped graphene: synthesis, characterization, and its potential applications. Acs Catal 2012;2(5):781–94.
[30] Lin ZY, Waller GH, Liu Y, Liu ML, Wong CP. 3D Nitrogen-doped graphene prepared by pyrolysis of graphene oxide with polypyrrole for electrocatalysis of oxygen reduction reaction. Nano Energy 2013;2(2):241–8.
[31] Yang SB, Feng XL, Wang XC, Mullen K. Graphene-based carbon nitride nanosheets as efficient metal-free electrocatalysts for oxygen reduction reactions. Angew Chem Int Ed 2011;50(23):5339–43.
[32] Lai LF, Potts JR, Zhan D, Wang L, Poh CK, Tang CH, et al. Exploration of the active center structure of nitrogen-doped graphene-based catalysts for oxygen reduction reaction. Energy Environ Sci. 2012;5(7):7936–42.
[33] Wang XQ, Lee JS, Zhu Q, Liu J, Wang Y, Dai S. Ammonia-treated ordered mesoporous carbons as catalytic materials for oxygen reduction reaction. Chem Mater 2010;22(7):2178–80.
[34] Poh HL, Simek P, Sofer Z, Pumera M. Sulfur-doped graphene via thermal exfoliation of graphite oxide in H_2S, SO_2, or CS_2 gas. ACS Nano 2013;7(6):5262–72.